Future Circular Collider

PUBLICATION

Overview of EIR design options: Deliverable D3.1

Seryi, Andrei (University of Oxford (GB)) *et al.*

30 January 2019

The research leading to this document is part of the Future Circular Collider Study

The electronic version of this FCC Publication is available
on the CERN Document Server at the following URL :
<http://cds.cern.ch/record/2655278

Grant Agreement No: 654305

EuroCirCol

European Circular Energy-Frontier Collider Study

Horizon 2020 Research and Innovation Framework Programme, Research and Innovation Action

DELIVERABLE REPORT

OVERVIEW OF EIR DESIGN OPTIONS

Document identifier:	EuroCirCol-P1-WP3-D3.1
Due date:	End of Month 15 (September 1, 2016)
Report release date:	30/08/2016
Work package:	WP3 (Experimental insertion region design)
Lead beneficiary:	UOXF
Document status:	RELEASED

Abstract:

This document describes the options of EIR design and collider layouts to be considered for further detailed studies. We primarily focus on factors leading to selection of the optimal L* parameter, describe the options considered and the presently selected value, as well as possible further optimization. We also describe studies performed with the present EIR optics, such as orbit correction, muon cross-talk between interaction regions, impact of synchrotron radiation as well as beam-beam effects.

The European Circular Energy-Frontier Collider Study (EuroCirCol) project has received funding from the European Union's Horizon 2020 research and innovation programme under grant No 654305. EuroCirCol began in June 2015 and will run for 4 years. The information herein only reflects the views of its authors and the European Commission is not responsible for any use that may be made of the information.

Delivery Slip

	Name	Partner	Date
Authored by	Andrei Seryi Rogelio Tomas	UOXF/JAI CERN	22/08/16
Edited by	Julie Hadre Johannes Gutleber	CERN	24/08/16
Reviewed by	Michael Benedikt Daniel Schulte	CERN	26/08/16
Approved by	EuroCirCol Coordination Committee		29/08/16

TABLE OF CONTENTS

1. EIR DESIGN OPTION

The optics of the Experimental Interaction Region (EIR) is integrated with the optics of the collider ring. The layout of the ring is shown in Figure 1 below. The current optics baseline is suitable for all design study work foreseen: radiation effects, design and optimization of machine detector interface (MDI), investigation of beam-beam interaction effects, dynamic aperture evaluation, effects of errors, as well as developing the procedures for transit from injection to collision optics. In the Table 1 below we describe the EIR optics options, in terms of L* and triplet dimensions, as in the following section describe our path to the presently selected optimal optics.

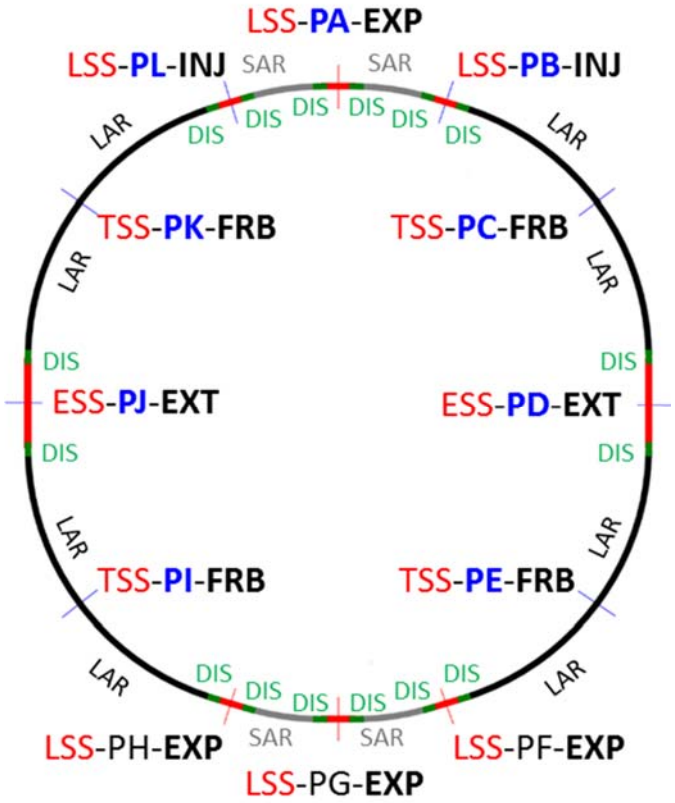

Figure 1: Layout of the collider ring.

Table 1 – List of central parameters of the different EIR options studied so far. In the following they will be identified by their L.*

	LHC	HL-LHC	FCC-hh			
L* [m]	23	23	46	36	61.5	45
$l_{Q1/Q3}$[m]	6.37	7.685	12.74	20	20.54	31.81
$l_{Q2a/b}$[m]	5.50	6.577	11.0	17.5	17.58	26.37
Quadrupole coil aperture diameter [mm]	70	150	62	100/115	140	205/248
Quadrupole gradient [T/m]	215	150	365	220/190	150	107/89
Normalized separation [σ_p]	9.4	12.5	12	12	14	15.2
Total length [m]	537.8	537.8	1075.6	1075.6	1400	1500

1.1. L* = 46 M

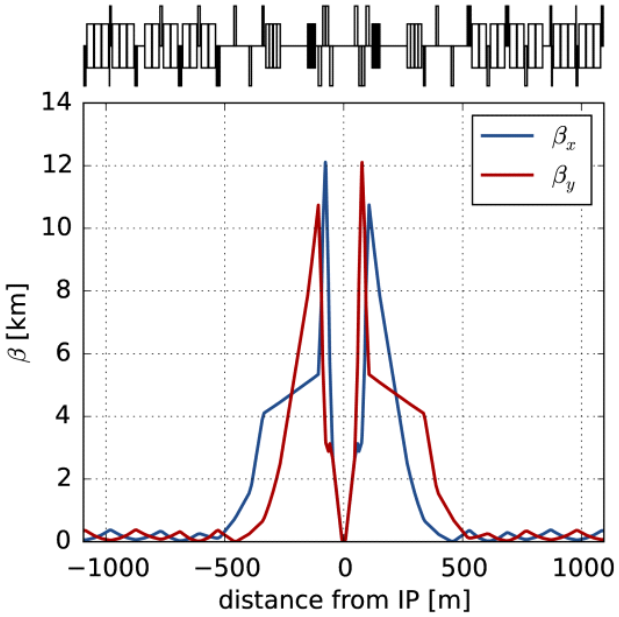

Figure 2: Optics of the scaled LHC IR including scaled dispersion suppressor

Being the first lattice layout for FCC-hh, the L* = 46 m option is a result of scaling the LHC IR lattice in length in order to cope with the increased beam rigidity. Using a scaling factor of 2 results in a constant beam stay clear at a doubled β* of 0.8 m. The resulting total length is 1075.6 m, which is shorter than the 1400 m specified in [1]. The separation section was modified to provide a separation of 300 mm. Unlike the HL-LHC, the LHC triplet has no dedicated shielding inside the quadrupoles to protect them from collision debris coming from the IP. This means in the lattice scaled from LHC with

constant beam stay clear, there is no space for shielding either, if the scaled β* of 0.8 m is to be maintained. The increase in centre-of-mass energy, proton-proton cross section and luminosity goals (peak and integrated) suggests an increase in energy deposition by about two orders of magnitude. This huge increase might pose a problem so FLUKA simulations were conducted to study the radiation load. Figure 3 shows the simulation results. The highest power density occurs at the end of Q1. With 230 mW/cm^3 it is about 60 times higher than the maximum power density in the LHC triplet and considerably above the assumed quench limits of Nb_3Sn (40 mW/cm^3) and NbTi (13 mW/cm^3) [2]. The maximum peak dose also occurs in Q1 and with about 2400 MGy per 3000fb^{-1} it is two orders of magnitude higher than the assumed lifetime limit for the present magnets of 30 MGy. A straight forward option to reduce the radiation load is shielding placed inside the quadrupoles, as it is done in HL-LHC already. Placing similar amounts of shielding inside the scaled triplet magnets will reduce the free aperture and limit the minimum β*. It is therefore unlikely that the baseline goal of β* = 1.1 m can be reached with sufficient shielding in this option.

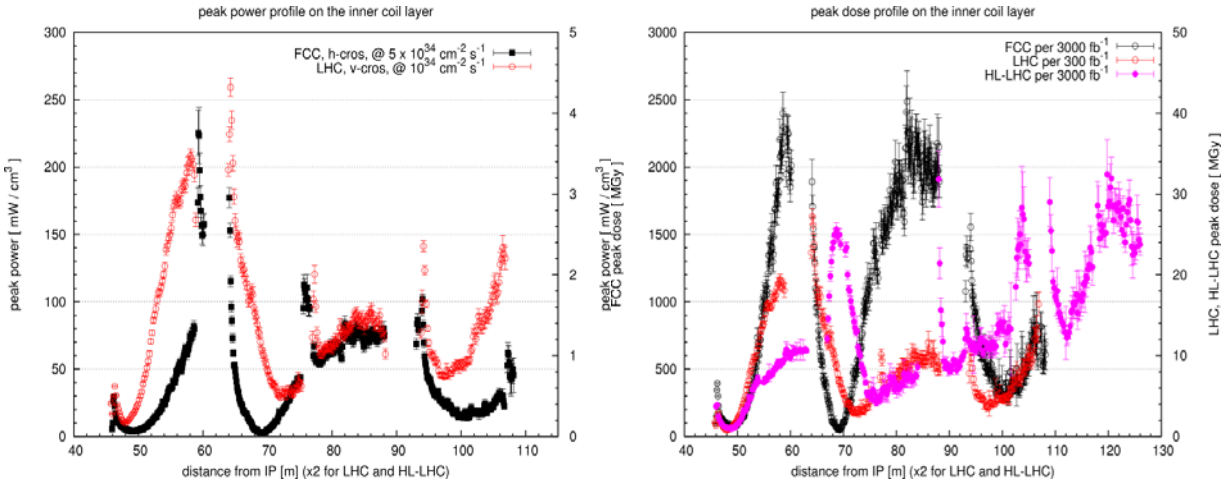

Figure 3: Peak power densities and peak doses for the L = 46 m lattice compared to LHC and HL-LHC*

1.2. L* = 36 M

In order to make space for the shielding, the HL-LHC lattice, having a triplet already 20 % longer than the LHC, was scaled by the factor of 2. After scaling, the triplet magnets were lengthened by an additional 30% in order to be able to decrease the gradients, increase the apertures and subsequently accommodate more shielding. Increasing the triplet length results in larger β functions. To keep this increase in reasonable limits, L* was reduced to 36 m. This counteracts the effect of the longer triplet partly but a net gain in the gradients is expected. The L* is not too far from to the upper limit of early detector design studies, suggesting a detector half-length of 25 to 40 m. FLUKA studies of the new lattice with continuous shielding layers of INERMET180 ranging from 0 mm to 20 mm are shown in Figure 5. The results show that, in order to get below a peak dose of 50 MGy, the region of technical feasibility, a shielding thickness of at least 15 mm is necessary.

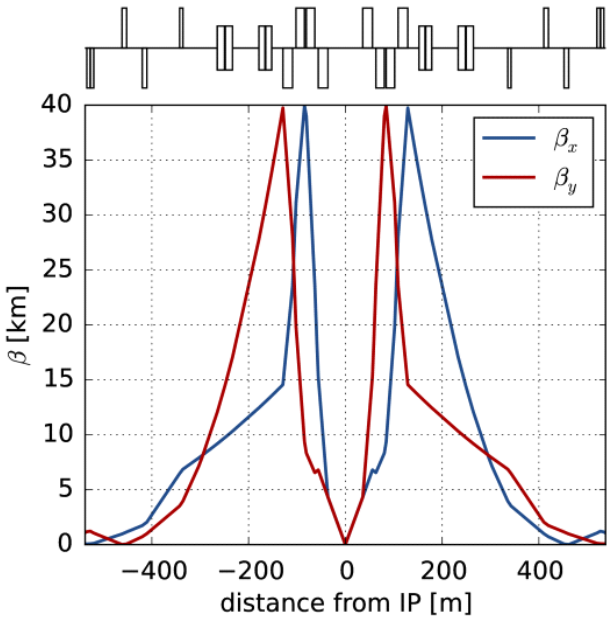

Figure 4: Optics of the L = 36 m lattice with β* = 0.3 m*

With this first specific figure, it is possible to refine the aperture model and the triplet matching in order to optimize the usage of available aperture and study the β* reach of a given lattice. When probing the minimum β*, we observed that Q1 happened to be about 20 % stronger than Q2 and Q3. Since the coil aperture of the triplet was defined by the strongest gradient, Q1 was limiting the aperture, while at the same time having the smallest β functions (see Figure 4). By using different apertures in Q1 and Q2/Q3 we can expect to get a better β* reach. In Figure 6 the minimum β* as a function of the required beam stay clear is plotted for both uniform apertures (all apertures defined by the strongest gradient in Q1) and for individual apertures.

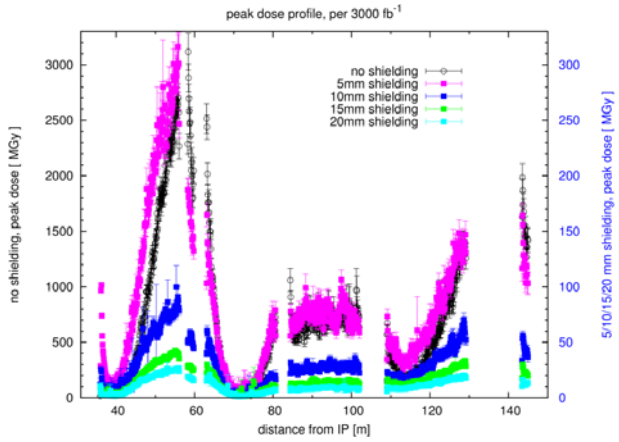

Figure 5: Peak dose for the L = 36 m lattice for different shielding thicknesses at 70 rad crossing angle and 100 mm coil aperture*

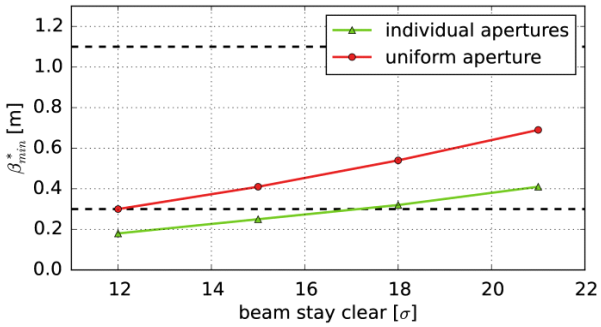

Figure 6: Minimum β of the L* = 36 m lattice as a function of the beam stay clear requirement.*

1.3. L* = 61 M

An alternative scaling factor of $\sqrt{\frac{50\ TeV}{7\ TeV}} \approx 2.67$ leaves gradients and apertures constant, allowing the reuse of existing magnet designs. The factor was applied to the HL-LHC lattice (version SLHC V3.1b), leading to L* = 61.5 m. The minimum β* is plotted in Figure 9. Comparing to L* = 36 m (Figure 6) shows that the minimum β* reachable in both lattices is the same. Although the relative impact of the shielding on the free aperture is smaller due to a larger coil aperture, the increased normalized separation prevented gains in the β* reach. The difference in the field at coil aperture (11 T in the L* =36 m option vs. 10.5 T for L* = 61 m) is a rather small effect in terms of minimum β*. FLUKA simulations with the L* = 61 m lattice (see Figure 8) show a peak dose about 20 % lower than in the L* = 36 m lattice. The main reasons for this are the larger coil apertures as well as the reduced gradient, limiting the particle losses in the defocusing planes. A counteracting effect comes from the larger crossing angle but the overall effect is a reduced load.

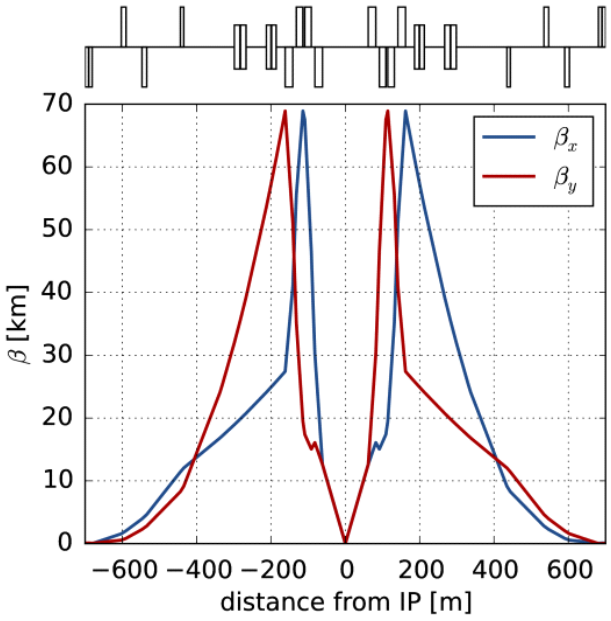

Figure 7: Optics of the L = 61 m lattice with β* = 0.3 m*

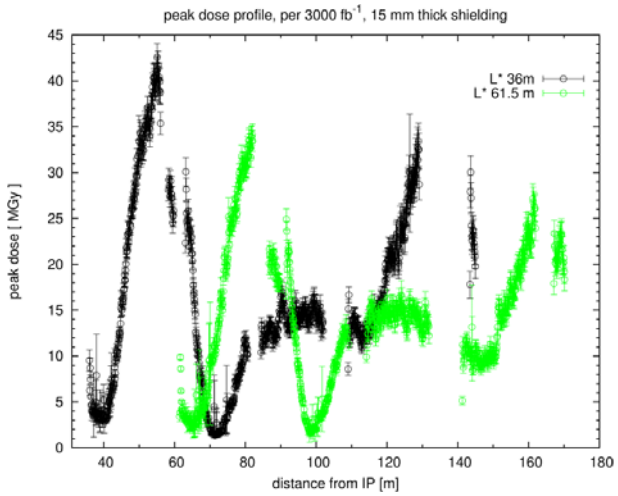

Figure 8: Comparison of the peak doses for the L = 36 m and L* = 61 m lattices.*

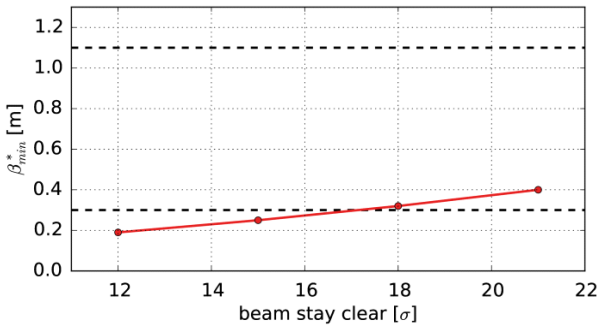

Figure 9: Minimum β of the L* = 61 m lattice as function of the beam stay clear requirement.*

1.4. L* = 45 M

Studies that scaled the L* = 36 m lattice and L* = 61 m lattice in length in order to investigate the behaviour of the minimum β* reachable suggested a strategy of choosing the smallest L* that does not restrict the detector design – to increase triplet length until dynamic aperture or chromaticity become the obstacles. The L* = 45 m lattice is the first lattice to implement this strategy along with constraints from a new detector design. A 10 Tm forward spectrometer requires a correction dipole right behind the detector. Shielding requirements and the TAS led to a minimum L* of 45 m. The triplet magnet lengths were increased by 50 % to improve on the minimum β*. Figure 11 shows the beam stay clear for various ambitious β* settings. When accepting a minimum beam stay clear of 12σ, β* can be pushed down to 0.05 m. For the "ultimate" β* = 0.3 m, the beam stay clear is 40 σ, a value much larger than necessary for collimation. It is possible to fill up the free aperture with additional shielding to reduce the radiation load further. If neither a smaller β*, nor beam stay clear or shielding increase are viable or necessary, the triplet should be shortened again in order to reduce the maximum β function, that will be driving the chromaticity and limit the dynamic aperture. Figure 14 shows the peak dose profile for the L* = 45 m scenario, both for vertical and horizontal crossing without the spectrometer, to compare with previous cases. The values are lower thanks to the significantly larger coil aperture. In the same plot, an optimized running scheme is shown, where the crossing plane and the vertical crossing angle polarity are switched during the run in order to distribute the radiation azimuthally.

In the plot on the right, the peak dose profile is presented for horizontal crossing in the case with a spectrometer. The actual dose distribution is significantly influenced by the presence of the latter and, in particular, the maximum dose is on the horizontal plane even for internal vertical crossing, spoiling the effectiveness of the crossing angle gymnastics discussed above. Still, the regular inversion of the spectrometer polarity has a natural beneficial effect, distributing the hot spot on the two sides of the horizontal plane and limiting it below 30 MGy for 3000 fb^{-1}.

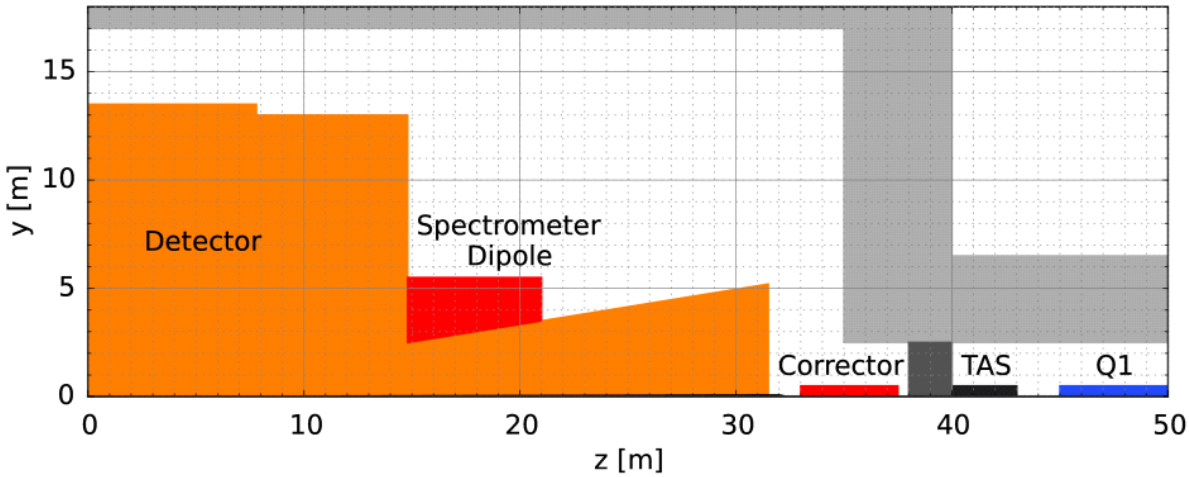

Figure 10: Schematic detector and IR layout leading to L = 45 m. The IP is located at (0,0).*

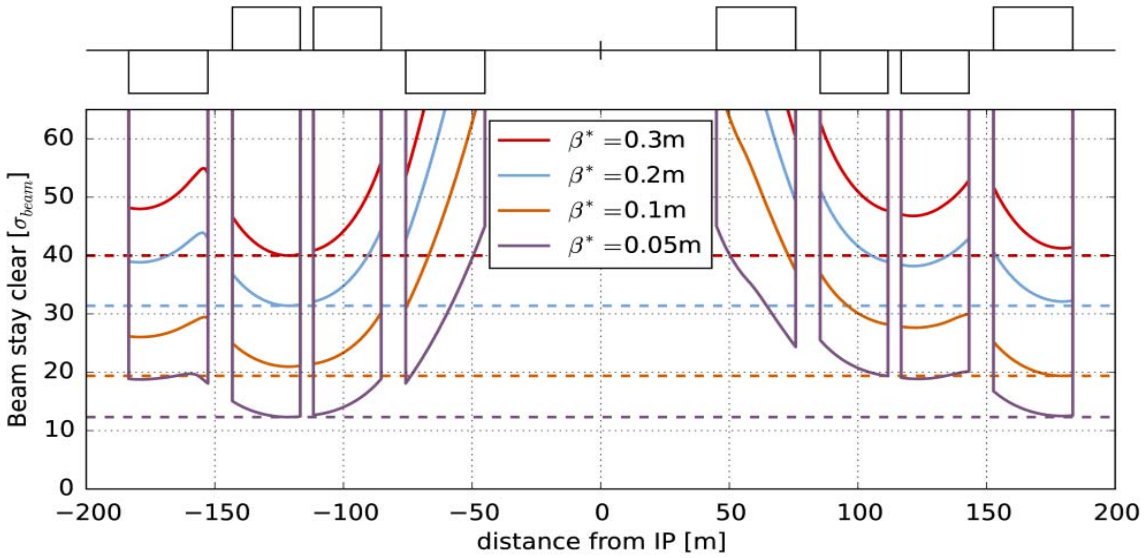

Figure 11: Beam stay clear of the L = 45 m lattice for various ambitious β* settings*

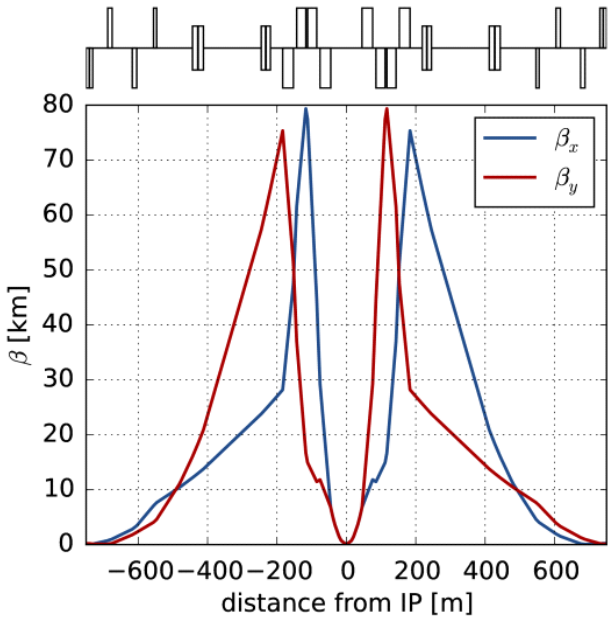

Figure 12: Optics for the L = 45 m lattice with β* = 0.3 m*

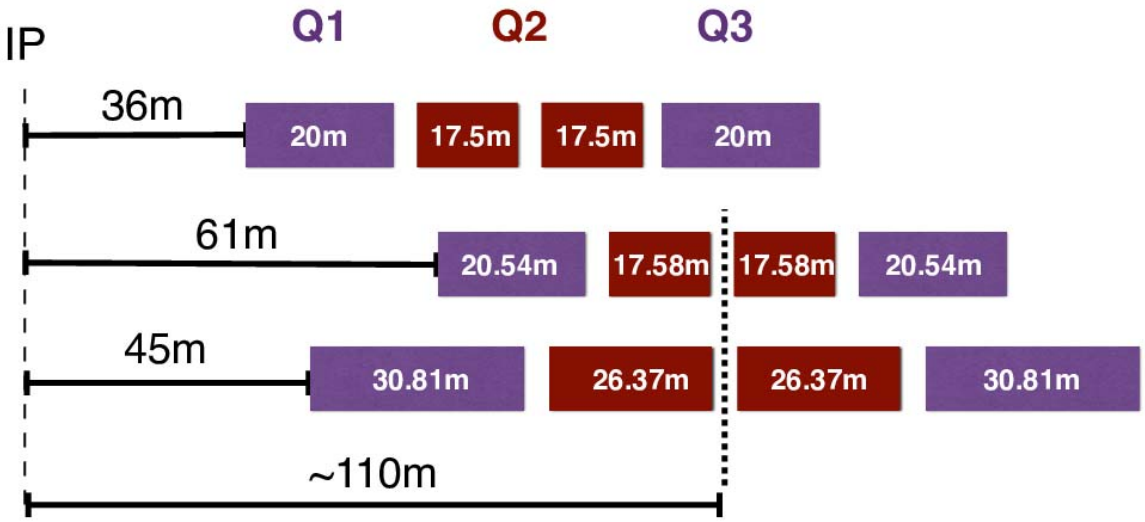

Figure 13: Length comparison of the 3 latest lattices.

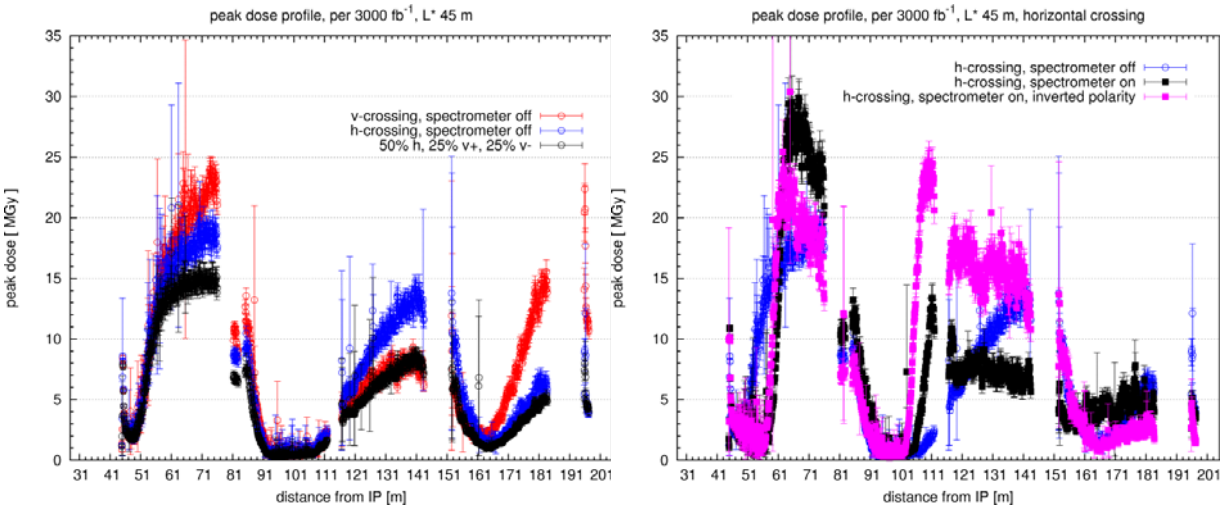

Figure 14: Peak dose distribution with spectrometer off (left) and on (right). The strong early deflection of the debris leads to a significant peak dose increase, most notably in Q1 and Q2a.

2. ORBIT CORRECTION SCHEME

The aim of the correction scheme is to control possible errors in the quadrupoles of the interaction region arising from possible misalignments or field errors while maintaining the crossing angle.

The correction scheme used is based on the HL-LHC scheme with correctors next to the quadrupoles closest to interaction points IPA and IPG (MQXD.A2, MQXC.3 and MQYY.4) as illustrated in Figure 15. These correctors will be used for both maintaining the crossing angle and to correct the orbit. The system also includes correctors next to the quadrupoles in the matching section and in the dispersion suppressor. A series of BPMs were also installed next to each corrector to monitor the orbit.

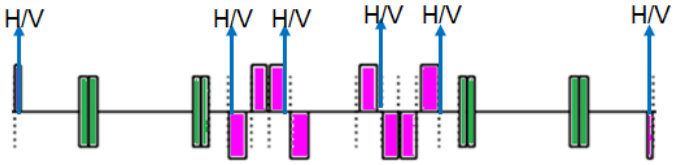

Figure 15: Layout of the correction scheme in the IR. The pink blocks represent the quadrupoles, the green blocks represent the dipoles, while the correctors and the BPM are represented by blue arrows and dotted lines respectively.

The correction procedure consists on assigning random errors to the magnets. The CORRECT method in MADX is then applied to find the appropriate strengths of the correctors necessary to restore the orbit. Once the correction is made, the strengths of the correctors and the maximum deviation from the orbit are stored. The procedure is repeated for 500 seeds. The output result is given by calculating the 90-percentile, meaning the value for which 90% of the distribution is included.

The results were done for different types of errors: quadrupole misalignments, field errors, tilt errors and combinations of the previous. The previous cases were repeated for different values of errors (with a Gaussian around 0.35 and 0.5) and for different optics (β^*=1.1 m and β^*=0.3 m). Figure 16 presents both the 90-percentile of the distribution for the maximum deviation and the maximum strength of the correctors.

As observed in the figures the correctors strengths do not present a problem given than for the worst case scenario the maximum corrector strength needed is of 1 Tm, which is achievable with the present technology. On the other side the maximum orbit deviation is quite small when applying tilt, field or quadrupole errors for the optics of β^*=1.1 m and even combining errors with the same optics the results look acceptable. The optics for β^*=0.3 m presents more challenging results, particularly for combined errors; however for the worst case scenario (0.5 misalignment error and 1 μrad tilt error) the 90-percentile of the maximum deviation is of 0.57 mm, if a tolerance of 0.5 mm is chosen the maximum deviation obtained for this case is just above this value.

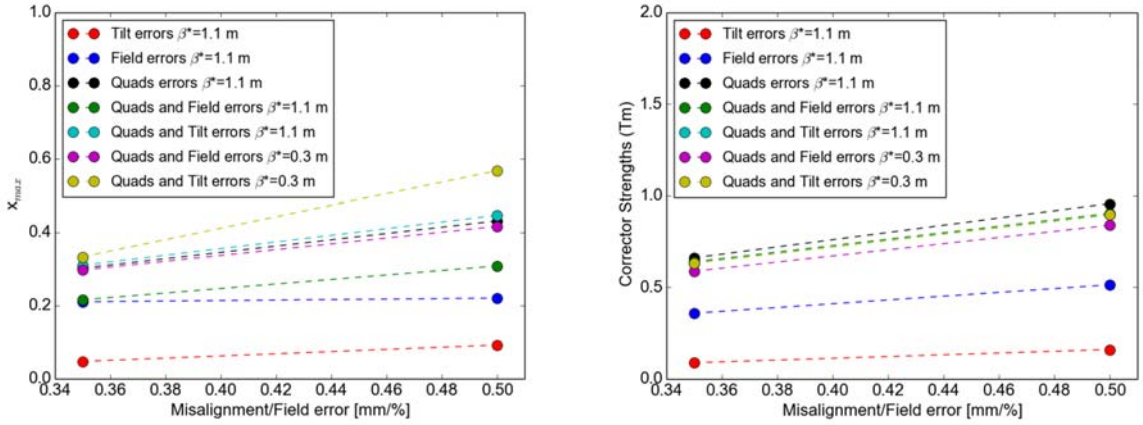

Figure 16: Results of the chromatic correction procedure for different types of errors. On the left the 90-percentile of the maximum deviation is presented while on the right the 90-percentile of the maximum strength of the corrector is given.

2.1. INNER TRIPLET OPTIMISATION

One important aspect of the IR is the size of the inner triplet since a shorter triplet takes up less space in the ring, is cheaper to construct, should reduce the chromaticity and might ease correction schemes. The current design of the FCC inner triplet is based on that of the LHC and was rescaled with energy and final drift length. The initial LHC design aimed primarily to minimise the beta function in the triplet.

The total length of the inner triplet in this design is 185 m and at a half crossing angle of 90 μrad and an ultimate β^* of 0.3 m the minimum beam stay clear is more than 40 σ. It is clear from this that the triplet can be further shortened and still maintain a beam stay clear larger than 12 σ, which is largely considered as the safe limit. Due to the large energy in the beam one must also, however, take into consideration the energy deposition in the magnets due to synchrotron radiation when optimising the design.

A python script was written that uses thin lenses to work out a figure of merit that approximates the beam stay clear for a large number of lens configurations. This is then used to identify a region with the highest potential beam stay clear in which a more precise scan of configurations is performed using thick lenses and the MADX aperture module. An example of the results of such a scan is shown in figure 17, it is put next to a slower scan made using MADX for comparison. The script gradually increases the total length of the inner triplet until the target of 12 σ beam stay clear is reached.

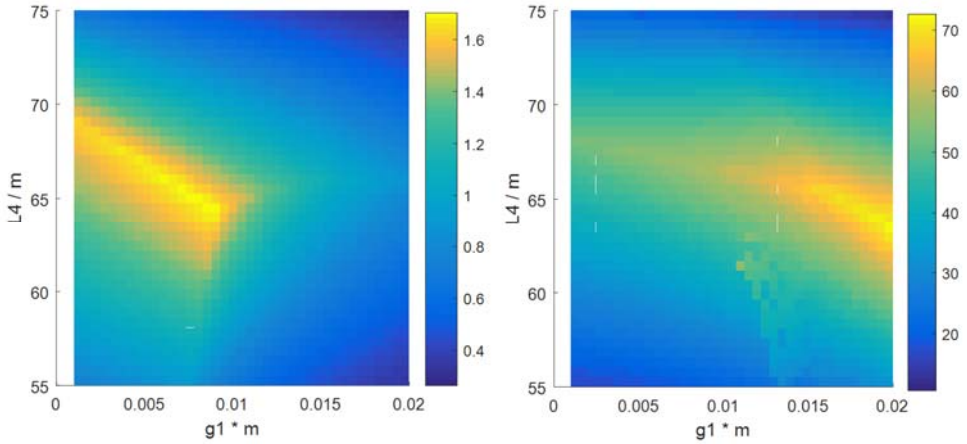

Figure 17: Figure of merit calculated using the fast thin lens method (left) and the beam stay clear using the MADX aperture model (right) for a range of different setups.

The optimum setup can then be easily integrated into the interaction region for matching and then into the entire ring. The python script offers great flexibility as changes to parameters such as the IP beam requirements, shielding thickness or spacing between magnets can easily be made and new optimum layouts can be found quickly. A first result of an optics produced by this code is shown in figure 18, the spacing between magnets have been reduced to 2 m and the entire triplet is 125 m long.

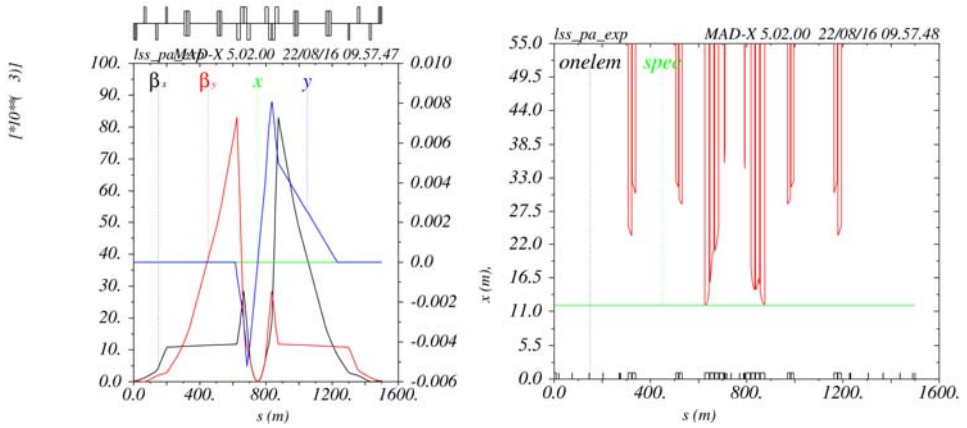

Figure 18:TWISS parameters and beam position (left) and beam stay clear (right) for a 125 m inner triplet.

2.2. RADIATION STUDIES

The triplet optimisation is being used to design a triplet that is as short as possible. This can then be integrated into the whole ring to be test features like chromaticity or beta beating and can also be simulated in FLUKA for radiation studies. From these tests the improvements, such as increasing the shielding can be suggested and included in a new run of the optimisation. This process is being iterated to find a design that fulfils all the requirements and is as short as possible. The magnets of the FLUKA model have been parametrized for a fast iteration.

3. EXPERIMENTAL CROSS TALK FROM MUON BACKGROUND

3.1. EXPERIMENTAL CROSS-TALK

With the 100 TeV c.m. proton-proton collisions at the FCC-hh, experimental cross-talk is a possible issue. In a first study we have investigated elastic and inelastic protons transported through the beam pipe, and muons through rock. The result of the overall study will have implications for experiments and potentially the collimator structure in the machine.

Using an L* of 45 m, and β* of 0.3 m with no crossing angle and normalised emittance of 2.2 μm, we generate particles at IPA and study particle flow to IPB, as representative of IPG to IPH. The upgraded version of DPMJET-III in FLUKA is used to generate proton-proton collision events at the FCC-hh c.m. energy.

It was found that for inelastic protons propagating forward of the IP, the highest losses occur in the inner triplet, and separation and recombination dipoles D1 and D2, which is consistent with findings from the FLUKA team [3]. A loss rate of 1 x 10^7 protons per second per metre was estimated at the start of the arc post IPA for ultimate parameters; this is an order of magnitude higher than the tentative agreed loss limit of 0.5 x 10^6 protons per second per metre, highlighting the need for possible mitigation of losses in this region. At a rate of 37 protons at IPB per beam crossing at ultimate settings, the inelastic protons may cause some background.

The rate of elastic protons at IPB per beam crossing is 85 at nominal, and 512 at ultimate settings. These protons have a spot size comparable to the nominal beam size, and will lead to emittance growth.

As a first approach an analytical investigation of the range of muons generated with DPMJET-III was performed. Muons are mostly produced through the decay of collision products, and thus were recorded 3 m from the IP in the forward direction. Around 4 x 10^5 muons were produced in the forward direction when generating 1 x 10^6 proton-proton collisions after 3 m. The maximum muon energy recorded was ~22 TeV. The range of these muons is shown in Figure 19, from which it is clear that no muons have the required energy to travel the 5.92 km distance between IPA and IPB. This analytical calculation does not include range straggling or stopping power fluctuations, thus a FLUKA model of the tunnel, as well as the rock that covers the chord between IPA and IPB will be used to investigate this in detail, as well as the possibility of muons being guided by the tunnel or vacuum pipe. Muons that enter the beam pipe from the IP will not travel far in the accelerator due to their rigidity.

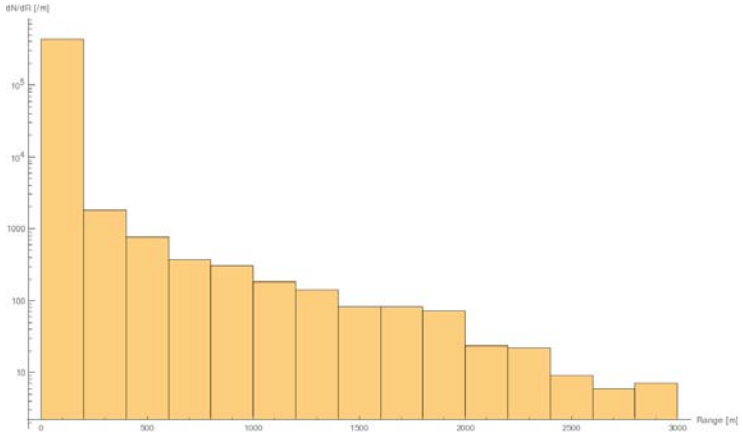

Figure 19: Analytical range of collision debris muons 3 m post IPA through standard rock. IPB is 5.92 km from IPA through rock.

The impact of crossing angle and the detector magnets on the detector cross-talk has yet to be checked, both the muon and proton calculations will benefit from the use of particle shower codes which are envisioned in the near future. The muon distribution at arbitrary distance from the IP will also be checked in order to provide the best range estimates, and FLUKA simulation optimisation.

3.2. FLUKA SIMULATIONS

Two models are used for the simulations. The first one includes the detector and has been provided by the FLUKA team. This model will be used to score muons after the tunnel rock. The muons at this point are mostly produced by the decay of the collision products. The second model is a modification of the triplet model made by the FLUKA team and used for energy deposition studies. In this model, shown in Figure 20, the tunnel has been enlarged until IPH and is surrounded by rock material. The muons produced after the experimental cavern will be tracked and scored in IPH. This will allow identification of the number of muons travelling through the rock, including those bounced back in the rock.

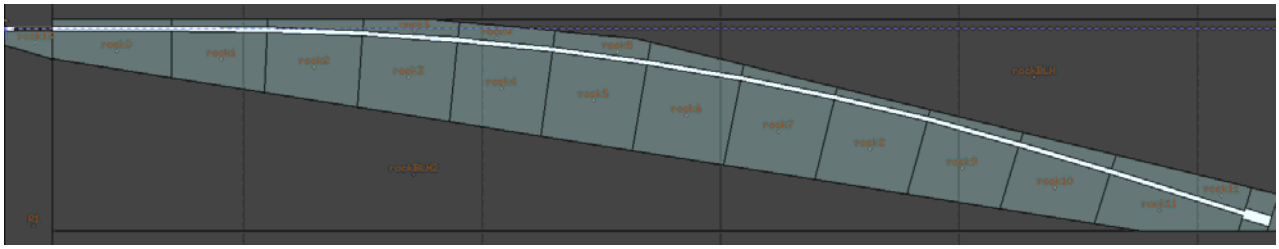

Figure 20: Horizontal cross section of the FLUKA model for the tunnel section IPG-IPH..

4. SYNCHROTRON RADIATION CONSIDERATIONS

A dedicated study for the evaluation of the synchrotron radiation in the interaction region for FCC-hh has started and is in progress. This study finds its motivation in the extremely high energy of the protons, being 50TeV, almost 7 times greater than in the case of LHC.

The effect of SR is important mainly in the arcs, where particles are bent, and where possible heating of the pipe can happen due to the emitted photons, and in the interaction region, where these photons can constitute a background to the detectors.

We focus in our study on the synchrotron radiation in the IR, to verify that the optics satisfies the detector's requirements from this point of view.

We performed our study for the baseline optics (fcc_hh_v6_45) and we plan to investigate different possible operating conditions, like with and without crossing angle, but also with horizontal and vertical beam displacement at the interaction point.

In order to evaluate the radiation effects in the detector, we focused our attention on the particles entering the interaction region (defined as "what is after the TAS") which originate from the last 2 bending magnets (D1-D2). To perform this study we used MDISim, [4]which is a set of C++/Root classes that allows to run MADX with the desired lattice, read the MADX output plotting the lattice, and to perform several calculations regarding SR (power radiated, number of emitted photons, critical energy for each element..) plotting it on the accelerator geometry.

We calculated a power of about 15-30 W entering the TAS, carried by some 10^10 photons with a mean energy of 300eV, demonstrating that SR is not expected to be an issue in the IR.

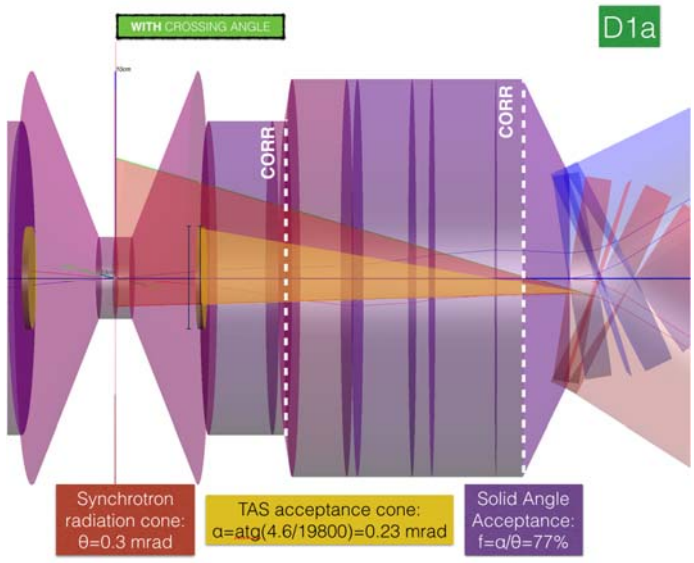

Figure 21: Example of the geometrical procedure used to evaluate the solid angle of SR coming from the bendings and entering the TAS. In this case (first bending, D1) the fraction of SR produced in the magnet that enter the TAS is 77%

To find these numbers, as a first step, we evaluated the solid angle with which SR photons emitted in those bending magnet can enter the TAS, using the graphical representation of the geometry given by MDISim. Then the percentage of photons entering the TAS was used to evaluate, starting from the SR parameters given by MDISim, the amount of power reaching the IR from the last two bending magnets.

This study has been performed in both cases, with or without the 80μrad crossing angle between the beams, which presence has a clear effect in the solid angle value.

The results are summarized in the following table for both cases.

el.	L (m)	B (T)	E_{crit} (keV)	P (W)	f_{TAS} W/O CA	f_{TAS} W CA (%)	P_{TAS} W/O CA (W)	P_{TAS} W CA (W)
D1a	12,5	-4,3	1,146	32	40	77	12,8	24,6
D1b	12,5	-4,3	1,146	32	0	0	—	—
D2a	15	3,6	0,955	27	15,3	16,7	4,1	4,5
D2b	15	3,6	0,955	27	0	0	—	—
D3	13,4	15,9	4,279	480	—		**17W**	**30W**

A similar study (solid angle evaluation and scaling of generated power) has been performed to evaluate the power hitting the 8m Beryllium pipe at the very center of the IR, which turned out to be about 2W.

These values for the generated SR power do not represent a major concern for the design of the accelerator. However, some other aspects should be addressed before considering this topic as closed.

In particular, the power inside the IR (and in the Beryllium pipe) is probably low, but is carried by a great number of low energy photons. The effect of optical reflection, absorption and transmission of these photons through Beryllium should then probably be studied to ensure they do not give rise to unexpected phenomena in the detectors.

Moreover, the contribution of SR coming from quadrupoles in the last triplet need to be considered. This study is presently still in progress. However, we can already say that we expect this contribution to be lower by about one order of magnitude than the one from bendings (relying on magnetic field considerations).

5. BEAM-BEAM EFFECTS

The beam-beam interaction is known to be an important factor limiting the performance reach of present particle colliders. The most important effects of beam-beam interactions are: a) the induced particle losses that decrease the beam lifetime and generate both high background load for physics experiments and elevated heat and radiation load on the collimation system; b) the degradation of beam quality, manifesting itself through the emittance blow-up that decreases the luminosity delivered to particle physics experiments.

Hence, the scope of this Task effort is to evaluate the expected impact of beam-beam interactions on the FCC machine, and to provide insight on possible limitations. These goals are achieved with the use of numerical simulations that are compared with experimental data where possible.

5.1 DYNAMIC APERTURE STUDIES

The investigation of beam-beam effects for the present LHC machine was mostly performed with the use of weak-strong approximation. This well-tested approach allows evaluating long-term particle stability in a very detailed accelerator model, and exploring wide ranges of the machine and beaming parameters. A number of computer simulation codes exist that have been under active development and in use for decades. The Task team chose to perform the beam-beam simulations for the FCC with the well-consolidated SixTrack code [4]. Sixtrack has been used successfully for the design of the LHC but represents also the code most benchmarked versus LHC data [5].

Studies have been performed on an L*=45 m lattice tracking particles at different betatron amplitudes for a total of 10^6 turns. At first only 5 phase space angles are used this will be improved in future studies to improve the resolution. The beam-beam interactions are simulated in a 4D fashion simulating full head-on collisions (crab crossing). No magnetic errors were available at the time of this study but they will consider later on. In all cases the maximum number of long ranges are considered (116 encounters).

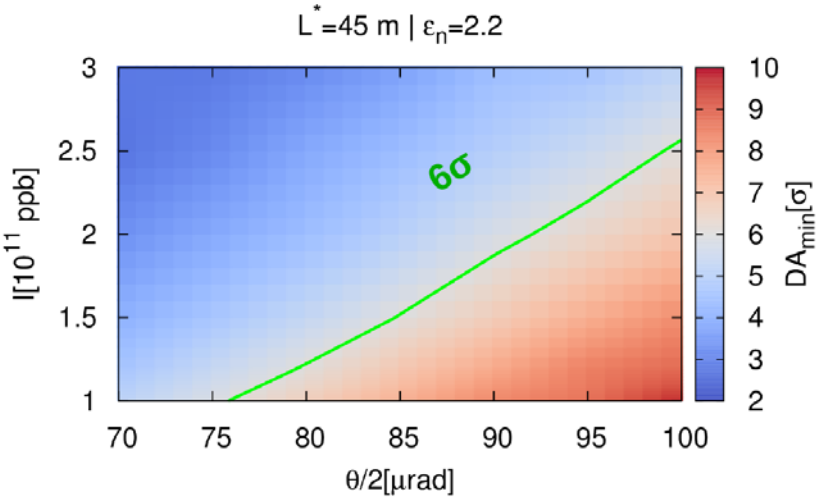

Figure 21: Dynamic aperture studies for a range of half crossing angles and intensities with full head on collisions at IPA and G. The isoline for 6σ is highlighted.

Figure 21 shows that for the baseline scenario with I=1 10^{11} ppb the half crossing angle needed to ensure a DA of 6 σ is θ/2~76 μrad, which translates into a normalized separation of d_{sep}~13 σ. This results is consistent with early simulations and analytical scaling laws [6].

As requested by the experiments the option of spectrometer is also analyzed with respect to its impact on the DA in the presence of beam-beam interactions. Similar simulations campaigns were launched turning out that negative polarity of the spectrometer is the preferred case since the long range are pushed further away so allowing for more relaxed crossing angles. For negative polarity the half crossing angle to ensure 6 σ DA is only θ/2~71 μrad while with positive is θ/2~87 μrad.

All studies have been performed using alternating crossing between the two experiments to profit of the long-range beam-beam passive compensation scheme for tune shifts and chromaticity changes as done for the LHC design. Future studies will also cover possible variations from this configuration with a possible modification of the required long-range separations defined in this report.

5.2 LONG RANGE COMPENSATION USING OCTUPOLES

Possible compensation schemes are at an early stage of study. The prove of principle and a parameter dependency study of these schemes i.e. compensation by multiple using octupole magnets and by the use of a wire, has started using the more flexible and stable optics files from the LHC and HL-LHC projects. The FCC optics are not yet at a mature stage.

The dynamic aperture is greatly limited by the long range encounters effect that enhance the tune spread for particles at large amplitudes. For this reason it is important to counteract this effect. Studies done in the framework of the HL-LHC study show for an optimized location of the octupoles it is possible to recover even 2 σ of DA by powering the octupoles with the correct polarity for the case of HL-LHC as shown in Figure 22. However differences have been observed with the LHC and are under investigation. A similar effect is expected for FCC and will provide important feedback to the optics design team to maximize the effects for the FCC configuration.

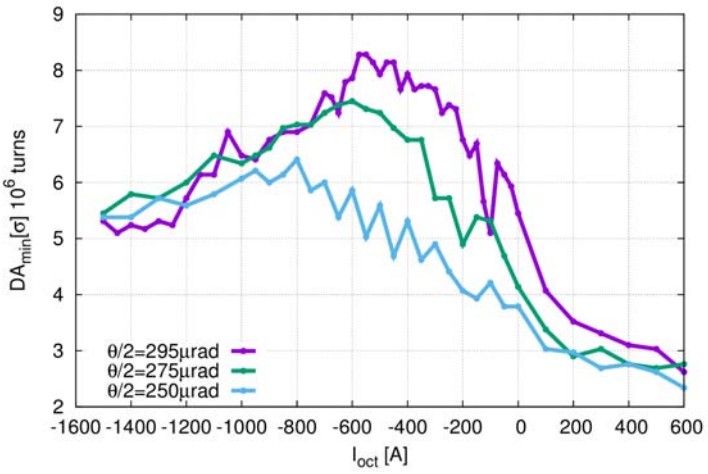

Figure 22: Dynamic aperture studies for a range of octupoles current and crossing angles for the HL-LHC nominal lattice. Improvements of DA is found for negative polarities of the octupoles.

6. SUMMARY AND IMPACT OF EACH OPTIONS

6.1. L* OPTIONS

During this study period we have considered various options for L* parameter ranging from 36 to 61 meters, as well as different configuration of the triplets. These options differ in terms of their ultimate reachable β* and differ in terms of radiation load on the inner triplet. We have concluded that the L*=46 m scaled from LHC does not provide space for radiation shielding and correspondingly would not allow to achieve even the baseline β* = 1.1 m. The L*=36m scaled from HL-LHC was better in terms of providing shielding and was shown to be able to achieve the baseline and ultimate β* = 0.3 m. Another version of optics scaled from HL-LHC, L*=61m demonstrated further improvements in terms of radiation load, while having the β* reach and maximal fields in the magnets about the same as in L*=36 m. The optics we eventually selected to be the present baseline is an intermediate version with L*=45 m – this value does not restrict the detector design, and the length of the triplet is allowed to be lengthened until limited by dynamic aperture or chromaticity. This design approach allows to significantly enhance the β* reach (down to 0.05 m) and/or create significant margin in stay-clear for reliable radiation protection. This optics option was selected as a baseline and further optimization and design study were based around it.

7. CLASSIFICATION AND RISK

7.1. RISKS OF DIFFERENT DESIGN OPTIONS

Among the optics options considered, the versions scaled from HL-LHC (L* of 36 and 61 m) have moderate risk and can be made to work for desired parameters, while having differences in terms of risks of their interference with detector, in particular. The presently selected baseline optics of L*=45 m represents the lowest risk in terms of energy deposition and β* reach. Dynamic aperture still needs further studies. All the other important factors considered – beam-beam effects, sensitivity to orbit errors, synchrotron radiation, are manageable in this design and are being further studied. The presently selected optics may reveal, with further studies, next levels of risks associated, for example, with manufacturability of long triplet, which may need to be split or somewhat shortened. Such an optimization of the optics is now going on in parallel with the detailed studies of the collider configuration based on the selected optics baseline.

8. CONCLUSIONS

We have described in this report the results of design studies towards the optimization of the optics of Experimental Interaction Region of FCC. We have evaluated several different options and compared their performance in terms of, in particular, β* reach and radiation load. We have come up with a design that satisfies the requirements of the project both for baseline and for the ultimate parameters, and are conducting further design study and optimizations around this baseline optics.

9. REFERENCES

[1] D. Schulte, "Preliminary collider baseline parameters," EuroCirCol-D1-1, 2015.

[2] I. B. A. O. B. M. L. a. L. R. G. Apollinari, High-Luminosity Large Hadron Collider (HL-LHC): Preliminary Design Report, Geneva: CERN, 2015.

[3] M. I. B. e. al, Assessment and Mitigation of the Proton-Proton Collision Debris Impact on the FCC Triplet, Busan: Proceedings of IPAC2016, 2016, pp. 1410 - 1414.

[4] Available at http://sixtrack.web.cern.ch/SixTrack/.

[5] M. Giovannozzi, «Proposed scaling law for intensity evolution in hadron storage rings based on dynamic aperture variation with time,» *Phys. Rev. ST Accel. Beams,* n° %1 15, 024001..

[6] S. P. a. B. Neuffer, «Beam-beam tuneshifts and spread in the SSC - Head on, long range and PACMAN conditions,» SSC-63, Dallas, USA, April 1986.

[7] "SixTrack website," available: cern.ch/sixtrack-ng.

10. ANNEX GLOSSARY

SI units and formatting according to standard ISO 80000-1 on quantities and units are used throughout this document where applicable.

ATS	Achromatic Telescopic Squeezing
BPM	Beam Position Monitor
c.m.	Centre of Mass
DA	Dynamic Aperture
DIS	Dispersion suppressor
ESS	Extended Straight Section
FCC	Future Circular Collider
FCC-ee	Electron-positron Collider within the Future Circular Collider study
FCC-hh	Hadron Collider within the Future Circular Collider study
FODO	Focusing and defocusing quadrupole lenses in alternating order
H1	Beam running in the clockwise direction in the collider ring
H2	Beam running in the anti-clockwise direction in the collider ring
HL-LHC	High Luminosity – Large Hadron Collider
IP	Interaction Point
IPA/IPG	Interaction Points housing the two main experiments
LHC	Large Hadron Collider
LAR	Long arc
LSS	Long Straight Section
MBA	Multi-Bend Achromat
Nb_3Sn	Niobium-tin, a metallic chemical compound, superconductor
Nb-Ti	Niobium-titanium, a superconducting alloy
RF	Radio Frequency
RMS	Root Mean Square
σ	RMS size
SAR	Short arc
SR	Synchrotron Radiation
SSC	Superconducting Super Collider
TAS	Target Absorber Secondaries
TSS	Technical Straight Section